

Review

Silicon Waveguide Optical Isolator with Directly Bonded Magneto-Optical Garnet

Yuya Shoji ^{1,*}  and Tetsuya Mizumoto ²

¹ Laboratory for Future Interdisciplinary Research of Science and Technology (FIRST),
Tokyo Institute of Technology, Tokyo 152-8550, Japan

² Tokyo Institute of Technology, Tokyo 152-8550, Japan; tmizumot@pe.titech.ac.jp

* Correspondence: shoji@ee.e.titech.ac.jp; Tel.: +81-3-5734-2578

Received: 15 January 2019; Accepted: 3 February 2019; Published: 12 February 2019



Featured Application: photonic integrated circuits and optical transceivers.

Abstract: Silicon waveguide optical isolators were fabricated by direct bonding of magneto-optical (MO) garnet. The technique allowed efficient MO phase shift owing to the use of single-crystalline garnet and negligibly thin interlayer on the silicon core layer. A Mach–Zehnder interferometer (MZI) provided optical isolation utilizing the MO phase shift. High isolation, wide bandwidth, and temperature-insensitive operations had been demonstrated by tailoring the MZI design. Also, transverse electric (TE)–transverse magnetic (TM) mode converters were integrated to control operating polarization. In this paper, we reviewed these progresses on silicon waveguide optical isolators.

Keywords: optical isolator; integrated optics devices; waveguides

1. Introduction

The growth of data centers demands high-speed and low-cost photonic integrated circuits (PICs) for optical transceivers and active optical cables. While the modulation frequency in an optical modulator is limited at ~50 GHz by the bandwidth of electronic circuits, higher bit-rate signals are achieved using multi-level phase and/or amplitude modulations and wavelength division multiplexing techniques. An optical isolator which prevents backward reflections is necessary for stable operations of laser diodes. However, no PIC integrated with a waveguide optical isolator has been realized yet.

There are several approaches for realizing optical isolation using nonlinear, electro-optical, and magneto-optical (MO) effects. Nonlinear effects can achieve nonreciprocity for optical signals between co- and counter-propagating with pump lights, though it puts a restriction for use in practical systems [1–4]. Electro-optical effects can break time-reversal symmetry by temporal-domain modulation depending on the propagation direction. The devices using an indirect bandgap transition due to traveling-wave modulation or pairs of modulators associated with passive phase shifter were demonstrated in silicon photonics platform [5–7]. The modulator or phase shifter should have longer interaction length and complex structures for effective isolation. Moreover, an RF high-power supply is required for the modulation. MO effects can realize optical isolation with simple structure and passive operation. The bottleneck is how to integrate a MO material on photonic platforms. MO garnets such as yttrium iron garnet (YIG) and cerium-substituted-YIG (Ce:YIG) have a larger MO effect and relatively low absorption loss in the infrared wavelength regions [8,9]. The single-crystalline YIG or Ce:YIG is typically grown on a gadolinium gallium garnet (GGG) substrate. Because of large mismatch of lattice constant and structure, growth of single-crystalline MO garnet on semiconductor has not been

realized yet. By use of seed layer or post annealing process, depositions of poly-crystalline Ce:YIG or terbium iron garnet (TIG) on semiconductor substrates have been investigated continuously [10,11].

MO isolators had been realized with direct bonding techniques. Ce:YIG dies were successfully bonded on silicon or compound semiconductor waveguide by surface-activating process. It enabled us to use an MO upper cladding layer of single-crystalline garnet with negligibly thin interlayer, which resulted in an effective MO interaction with propagating light. A nonreciprocal phase shift (NPS) was a direction-dependent propagation constant because of the first-order MO effect induced in the transverse magnetic (TM) mode. A Mach–Zehnder interferometer (MZI) or a ring resonator with the MO cladding layer allowed a nonreciprocal optical propagation. A ring resonator enabled small footprint, whereas its narrow operating wavelength was sensitive to temperature and fabrication errors. Huang et al. and Pintus et al. formed a planar spiral electromagnet on a ring resonator, which provided external magnetic field for the MO effect as well as controlled the device temperature by Joule heating [12,13]. An MZI configuration was relatively robust for temperature and fabrication errors as long as they were balanced between the two arms. Therefore, the operation bandwidth could be wider.

Shoji et al. firstly reported a Si MZI-based isolator in 2008 [14]. After that, they have demonstrated MZI-based isolators with an MO upper cladding layer having higher isolation, wider bandwidth, and temperature-insensitive operations [15–17]. In this article, we present an overview of the progress of MZI-based silicon waveguide isolator. The operating polarization is TM mode because NPS is induced in the TM mode for layered waveguide structures. We then present an integration of transverse electric (TE)–TM mode converter [18]. Finally, we discuss the possibility of low insertion loss.

2. Device Structure and Operation Principle

Figure 1 shows schematic of an MZI isolator with Si waveguides and Ce:YIG upper cladding layer. It has nonreciprocal phase shifters in the two arms and a phase bias in one of the arms. Since NPS caused a direction-dependent propagation constant, phase differences were nonreciprocal when external magnetic fields in anti-parallel directions were applied transversely to the light propagation along L_{NPS} . In addition, the two arms were slightly asymmetric by the length L_{RPS} , which provided reciprocal phase bias. Nonreciprocal and reciprocal phase differences are designed with the waveguide lengths as

$$\theta_{\text{NPS}} = (\beta_+ - \beta_-)L_{\text{NPS}} = \mp \frac{\pi}{2}, \quad (1)$$

$$\theta_{\text{RPS}} = \beta L_{\text{RPS}} = \frac{\pi}{2} + 2m\pi, \quad (2)$$

where β_+ and β_{\pm} are slightly different propagation constants of two arms due to the NPS, β is the propagation constant at the phase bias, m is an integer determined by L_{RPS} . The sign of θ_{NPS} is minus and plus for forward and backward directions, respectively. In the forward direction, light launched to the input port was transmitted to the output port by a constructive interference, because the total phase difference between the two arms was in-phase. In the backward direction, light coming back to the output port was radiated to the side ports of the input side by a destructive interference, because the total phase difference was out-of-phase. In this way, an optical isolation was achieved. Forward and backward transmittance between the input and output ports is given by

$$T_{\text{for,back}} = \cos^2\left(\frac{\theta_{\text{RPS}} \mp \theta_{\text{NPS}}}{2}\right), \quad (3)$$

where 3-dB couplers are assumed to work ideally.

Si waveguides were fabricated on a silicon-on-insulator (SOI) wafer by an electron-beam lithography and reactive ion etching. In order to ensure sufficient area of top Si layer for bonding, a 2.5- μm -wide Si layer beside the waveguide was removed as a side cladding region. The single-crystalline Ce:YIG grown on substituted-GGG wafer was cut into a 1.5-mm square die and bonded on the Si waveguide

by surface-activated bonding. The detailed process was described in [19]. Figure 2 shows a microscopic image of a fabricated MZI isolator. Though the whole MZI pattern was covered by the Ce:YIG die, an effective device footprint was about 500- μm -wide square.

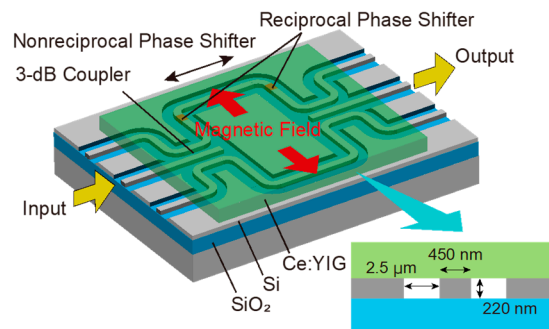


Figure 1. Schematic of Mach–Zehnder interferometer (MZI)-based optical isolator with magneto-optical (MO) upper cladding layer. Si waveguides are 450-nm wide and 220-nm high. 3×2 couplers function as 3-dB power splitter and combiner with directional coupling among three adjacent waveguides.

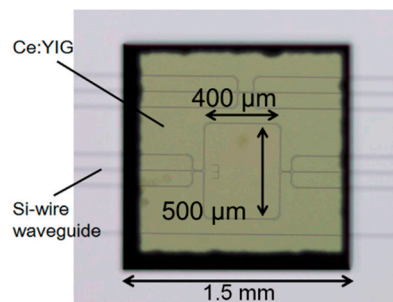


Figure 2. Microscopic image of fabricated MZI isolator on a silicon-on-insulator (SOI) platform. A 1.5-mm square die of cerium-substituted-YIG (Ce:YIG)/substituted-GGG is directly bonded on the Si waveguide. Two MZI arms are separated 500- μm away to apply external magnetic field in anti-parallel directions with a permanent magnet.

3. Operation Bandwidth

Although the MZI isolator was designed at a specific center wavelength, phase differences of MZI had a wavelength dependence. Typically, refractive indices of materials and MO effect decreased as wavelength became longer. The phase differences θ_{NPS} and θ_{RPS} decreased as well. Then, an MZI had a resonant spectrum with periods of in- and out-of-phase, the so-called free-spectral range (FSR). When a FSR was wider, the MZI isolator provided a higher isolation for the wider wavelength range. The integer m in Equation (2) determined the resonant period, and was designed by L_{RPS} . Figure 3 shows the relation between m and 20 dB isolation bandwidth. Smaller m and shorter L_{RPS} achieved a wider bandwidth, while it needed a precise fabrication of waveguide dimensions. Figure 4 shows measured transmission spectra of an MZI isolator fabricated with the length L_{RPS} of 3.7 μm , which corresponds to $m = 5$. An optical isolation over 20 dB was obtained at 8-nm wavelength range. The transmittance included ~ 20 dB coupling loss between the fiber and waveguide for two facets by edge coupling. The insertion loss of 13 dB was mainly due to the scattering and reflection at Ce:YIG and air cladding regions' boundaries.

Further wideband operation was possible by focusing on the backward operation [20]. In this scheme, θ_{NPS} and θ_{RPS} were designed $\pi/2$ and $3\pi/2$, respectively, so that they were subtracted for the backward operation. When the wavelength dependences of $\theta_{\text{NPS}}(\lambda)$ and $\theta_{\text{RPS}}(\lambda)$ had similar slopes, the deviations from the designed quantities cancelled each other. Consequently, the wavelength dependence is flat as shown in Figure 5. The slope of phase difference was adjusted by changing the

width and length of two arms. If 3-dB couplers worked ideally in a wide wavelength range, an optical isolator could operate for 1.31 and 1.55 μm [21].

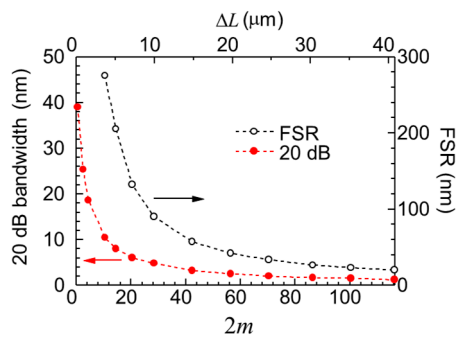


Figure 3. Free-spectral range (FSR) and 20-dB isolation bandwidth of an MZI isolator as a function of integer m of reciprocal phase bias.

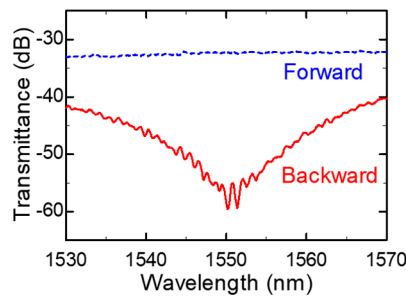


Figure 4. Measured transmission spectra of MZI isolator with a reciprocal phase shifter length L_{RPS} of 3.7 μm .

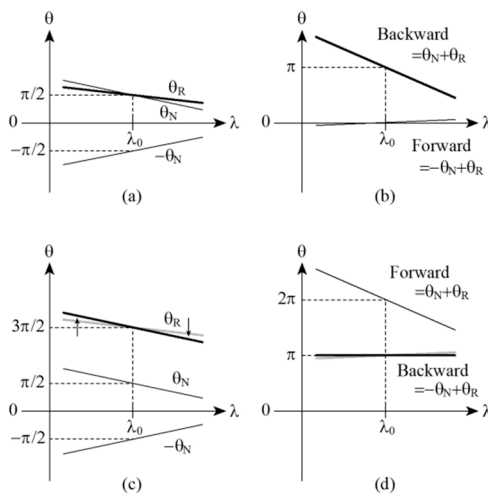


Figure 5. Wavelength dependence of nonreciprocal and reciprocal phase differences, θ_N and θ_R , respectively, of MZI isolator with (a,b) conventional design and (c,d) wideband design.

4. Temperature-Insensitive Operation

Since an optical isolator was placed near an optical active device to prevent backward reflections, the temperature change induced by the optical active device was unavoidable. We then investigated temperature dependence of the MZI isolator [17]. The temperature dependence of Si and SiO₂ was well-known, while that of Ce:YIG was not studied yet. The refractive index and Faraday rotation coefficient of Ce:YIG were $n = 2.2$ and $\theta_F = -4500^\circ/\text{cm}$, respectively, at room temperature and 1550 nm wavelength. A temperature change caused the wavelength shift in the MZI isolator owing to the

temperature dependence of the refractive indices (dn/dT) and MO effect ($d\theta_F/dT$) of the composed materials. By analyzing the measured temperature dependence of the MZI isolator, the unknown parameters of Ce:YIG film were determined as $dn/dT = 9.1 \times 10^{-5}/K$ and $d\theta_F/dT = 44^\circ/cm/K$. These indicated that the refractive index increased and the MO effect became weak at a higher temperature.

Temperature-insensitive operation of MZI isolator was proposed by cancelling the temperature dependence of phase differences $\theta_{NPS}(T)$ and $\theta_{RPS}(T)$. At a higher temperature, $\theta_{NPS}(T)$ decreased due to the decrease in the MO effect, whereas $\theta_{RPS}(T)$ increased due to the increase in the refractive indices, as described by the following equations.

$$\frac{d\theta_{NPS}}{dT} = \frac{d\Delta\beta}{dT} L_{NPS}, \tag{4}$$

$$\frac{d\theta_{RPS}}{dT} = \frac{dn_{eff}}{dT} k L_{RPS}, \tag{5}$$

where k is the wave number. An MZI was designed so that these temperature dependencies cancelled each other in the backward operation. Figure 6 shows the calculated temperature dependence of the total phase difference in an MZI as a function of L_{RPS} . They were plotted in dots because L_{RPS} had to satisfy Equation (2) for integer m . It was found that the temperature dependence of total phase difference was zero at a specific L_{RPS} . To verify the concept, MZI isolators having several L_{RPS} were fabricated and characterized by changing the substrate's temperature. Figure 7 shows the measured transmission spectra of an isolator with $L_{RPS} = 20.51 \mu m$. In the forward direction, the spectra changed due to the temperature change. However, in the backward direction, only slight changes were observed in a temperature range of 20–60 °C. The difference in L_{RPS} from that predicted in Figure 6 is owing to some dimensional errors in the fabrication process and possible differences between the actual optical properties used in the calculation.

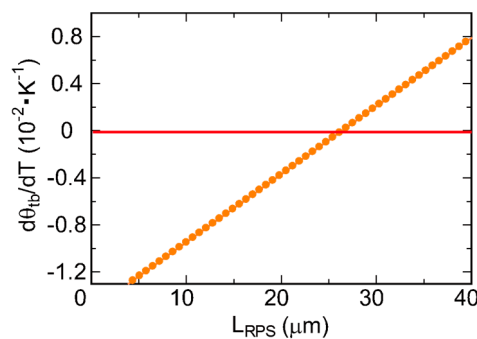


Figure 6. Calculated temperature dependence of the total phase difference on the length of reciprocal phase shift L_{RPS} . Red line indicates the point to be zero.

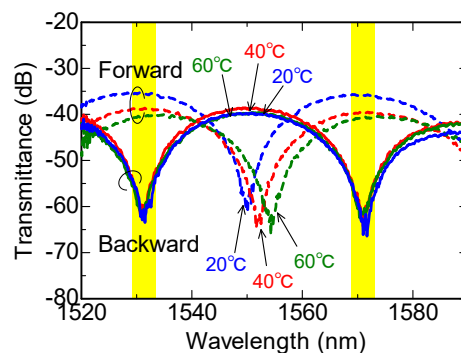


Figure 7. Measured transmission spectra of the fabricated MZI isolator designed for temperature-insensitive operation.

5. Integration of TE–TM Mode Converter

Only the TM mode experienced the NPS in the configuration with vertically asymmetric waveguide and horizontal magnetization. An NPS was obtained for TE modes when the MO material was placed in a horizontally asymmetric manner and subjected to vertical magnetization [22–25]. However, it required complicated fabrication processes or direct deposition of the MO material [10,11]. An alternative approach to achieve isolator operation for the TE mode input was to integrate TE–TM mode converters on the same waveguide platform [26]. Here, we presented a configuration of TE–TM mode converter compatible with the fabrication process using a direct bonding technique [18]. A polarization rotator was integrated at the input waveguide of an MZI isolator. The configuration allowed not only input light of TE mode to go through but also to block backward reflections of both the TE and TM modes.

Figure 8a shows the TE–TM mode converter consisting of two parallel waveguides. Because of air cladding waveguide without any prominent structure on the top Si, the photonic circuit was consistent with an optical isolator fabricated by direct bonding. The air cladding broke the vertical asymmetry, which was necessary for conversion between TE and TM modes. The two parallel waveguides with different width supported TE_0 , TE_1 , and TM_0 modes. The waveguides were then designed so that TE_1 and TM_0 modes had almost the same propagation constant. The TE input light injected into the narrow waveguide was efficiently converted into the TE_1 mode. After propagating a half-beat length L_π between the TE_1 and TM_0 modes, the light was converted to the TM_0 mode and output to the wide waveguide. By using a mode solver with finite element method, L_π was calculated to be $10.2 \mu\text{m}$ when the two waveguide widths and gap were 630, 285, and 95 nm, respectively. A fabricated mode converter exhibited a mode conversion efficiency of 90%.

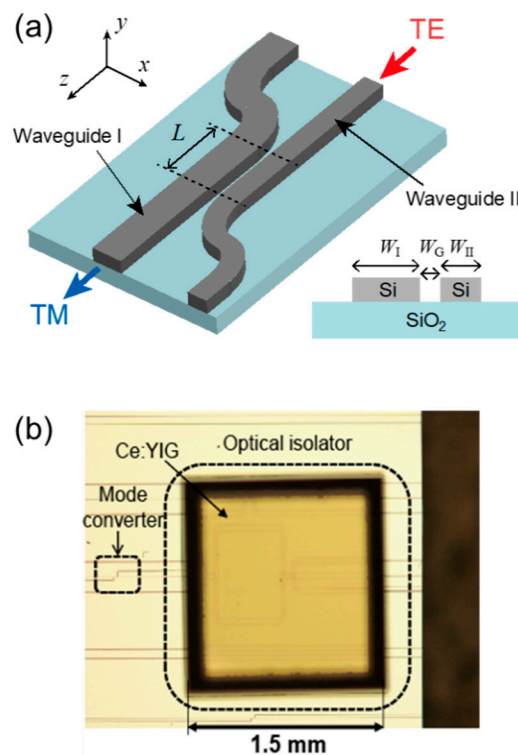


Figure 8. (a) Transverse electric (TE)–transverse magnetic (TM) mode converter consisting of two parallel waveguides. (b) Microscopic image of fabricated MZI optical isolator integrated with mode converter.

Figure 8b shows the microscopic image of a fabricated MZI isolator integrated with the TE–TM mode converter at the input side. A $100\text{-}\mu\text{m}$ -long tapered waveguide connected the wide waveguide

of mode converter to the 450-nm-wide input waveguide of MZI isolator. The polarization of input light was adjusted to the TE mode, whereas that of backward reflections was unpolarized. The backward TM mode can be eliminated in the MZI isolator by the MO effect. The backward TE mode was also eliminated by the following two structural effects. The directional coupler in the MZI isolator had strong polarization dependence. It operated as 3-dB splitter and combiner for the TM mode, whereas it gave a higher loss for the TE mode. The TE–TM mode converter showed asymmetry in the input and output waveguides. The backward TE light injected to the wide waveguide was almost coupled to the TE₀ mode; therefore, it was neither converted to the TM mode nor coupled to the narrow waveguide. The integrated isolator was characterized to demonstrate a maximum isolation of 26.7 dB for the TE mode input and TM mode backward lights.

6. Conclusions

We reviewed the progress on MZI optical isolators fabricated by direct bonding. The compact footprint on a silicon platform enabled high isolation at the peak of resonant spectra. The device structure and operation principle were described. The operation bandwidth related to the phase difference in the MZI was discussed. Next, demonstration of temperature-insensitive design and operation was presented. Finally, MZI isolator integrated with a TE–TM mode converter was presented. The remaining problem was insertion loss. The inherent loss of the MZI isolator was related to the Ce:YIG upper cladding region. An absorption loss of Ce:YIG can be minimized by reducing the Ce:YIG length along the light propagation to the minimum for achieving just a $\pi/2$ phase difference. There were scattering and reflection losses owing to mode mismatch at the boundary between Ce:YIG and air cladding regions. The loss was larger for the TM mode than for the TE mode because of the mode field distributions. Therefore, the scattering and reflection losses were mitigated so that light propagated as the TE mode at the boundaries. New configurations of optical isolator had been proposed using TE–TM mode converter to achieve this [27,28]. The insertion loss can be ~3 dB if other excess losses were resolved.

Author Contributions: Conceptualization, Y.S. and T.M.; methodology, Y.S. and T.M.; software, Y.S.; validation, Y.S.; formal analysis, Y.S.; investigation, Y.S.; resources, T.M.; data curation, Y.S.; writing—original draft preparation, Y.S.; writing—review and editing, T.M.; visualization, Y.S.; supervision, T.M.; project administration, T.M.; funding acquisition, T.M.

Funding: This study was supported by MIC/SCOPE #162103103; JST Core Research for Evolutional Science and Technology (CREST) #JPMJCR15N6 and #JPMJCR18T4; JSPS KAKENHI #16K06295; and TEPCO Memorial Foundation.

Conflicts of Interest: The authors declare no conflict of interest.

References

1. Krause, M.; Renner, H.; Brinkmeyer, E. Optical isolation in silicon waveguide based on nonreciprocal Raman amplification. *Electron. Lett.* **2008**, *44*, 691–693. [[CrossRef](#)]
2. Shi, Y.; Fan, S. Limitation of nonlinear optical isolators due to dynamic reciprocity. *Nat. Photonics* **2015**, *9*, 388–392. [[CrossRef](#)]
3. Dong, C.; Shen, Z.; Zou, C.; Zhang, Y.; Fu, W.; Guo, G. Brillouin-scattering-induced transparency and non-reciprocal light storage. *Nat. Commun.* **2015**, *6*, 6193. [[CrossRef](#)] [[PubMed](#)]
4. Wang, K.; Gao, S.; Wang, Y.; Nirmalathas, A.; Lim, C.; Alameh, K.; Skafidas, E. Four-wave-mixing-based silicon integrated optical isolator with dynamic non-reciprocity. *IEEE Photonics Technol. Lett.* **2016**, *28*, 1739–1742. [[CrossRef](#)]
5. Yu, Z.; Fan, S. Complete optical isolation created by indirect interband photonic transitions. *Nat. Photonics* **2009**, *3*, 91–94. [[CrossRef](#)]
6. Lira, H.; Yu, Z.; Fan, S.; Lipson, M. Electrically driven nonreciprocity induced by interband photonic transition on a silicon chip. *Phys. Rev. Lett.* **2012**, *109*, 033901-1-5. [[CrossRef](#)]
7. Doerr, C.; Chen, L.; Vermeulen, D. Silicon photonics broadband modulation-based isolator. *Opt. Express* **2014**, *22*, 4493–4498. [[CrossRef](#)]

8. Gomi, M.; Satoh, K.; Abe, M. Giant Faraday rotation of Ce-substituted YIG films epitaxially grown by RF sputtering. *Jpn. J. Appl. Phys.* **1988**, *27*, L1536–L1538. [[CrossRef](#)]
9. Shintaku, T.; Tate, A.; Mino, S. Ce-substituted yttrium iron garnet films prepared on Gd₃Sc₂Ga₃O₁₂ garnet substrates by sputter epitaxy. *Appl. Phys. Lett.* **1997**, *71*, 1640–1642. [[CrossRef](#)]
10. Sun, X.; Du, Q.; Goto, T.; Onbasli, C.; Kim, D.; Aimon, N.; Hu, J.; Ross, C. Single-step deposition of cerium-substituted yttrium iron garnet for monolithic on-chip optical isolation. *ACS Photonics* **2015**, *2*, 856–863. [[CrossRef](#)]
11. Dulal, P.; Block, A.; Gage, T.; Haldren, H.; Sung, S.; Hutching, D.; Stadler, B. Optimized magneto-optical isolator designs inspired by seedlayer-free terbium iron garnet with opposite chirality. *ACS Photonics* **2016**, *3*, 1818–1825. [[CrossRef](#)]
12. Huang, D.; Pintus, P.; Zhang, C.; Shoji, Y.; Mizumoto, T.; Bowers, J. Electrically driven and thermally tunable integrated optical isolators for silicon photonics. *IEEE J. Sel. Top. Quantum Electron.* **2016**, *22*, 4403408. [[CrossRef](#)]
13. Pintus, P.; Huang, D.; Zhang, C.; Shoji, Y.; Mizumoto, T.; Bowers, J. Microring-based optical isolator and circulator with integrated electromagnet for silicon photonics. *J. Lightw. Technol.* **2017**, *35*, 1429–1437. [[CrossRef](#)]
14. Shoji, Y.; Mizumoto, T.; Yokoi, H.; Hsieh, I.-W.; Osgood, R.M., Jr. Magneto-optical isolator with silicon waveguides fabricated by direct bonding. *Appl. Phys. Lett.* **2008**, *92*, 071117. [[CrossRef](#)]
15. Shoji, Y.; Mizumoto, T. Magneto-optical non-reciprocal devices in silicon photonics. *Sci. Technol. Adv. Mater.* **2014**, *15*, 014602. [[CrossRef](#)] [[PubMed](#)]
16. Shoji, Y.; Shirato, Y.; Mizumoto, T. Silicon Mach-Zehnder interferometer optical isolator having 8 nm bandwidth for over 20 dB isolation. *Jpn. J. Appl. Phys.* **2014**, *53*, 022202. [[CrossRef](#)]
17. Furuya, K.; Nemoto, T.; Kato, K.; Shoji, Y.; Mizumoto, T. Athermal operation of a waveguide optical isolator based on canceling phase deviations in a Mach-Zehnder interferometer. *J. Lightw. Technol.* **2016**, *34*, 1699–1705. [[CrossRef](#)]
18. Shoji, Y.; Fujie, A.; Mizumoto, T. Silicon waveguide optical isolator operating for TE mode input light. *J. Sel. Top. Quantum Electron.* **2016**, *22*, 4403307. [[CrossRef](#)]
19. Shoji, Y.; Ito, M.; Shirato, Y.; Mizumoto, T. MZI optical isolator with Si-wire waveguides by surface-activated direct bonding. *Opt. Express* **2012**, *20*, 18440–18448. [[CrossRef](#)]
20. Shoji, Y.; Mizumoto, T. Wideband design of nonreciprocal phase shift magneto-optical isolators using phase adjustment in Mach-Zehnder interferometer. *Appl. Opt.* **2006**, *45*, 7144–7150. [[CrossRef](#)]
21. Shoji, Y.; Mizumoto, T. Ultra-wideband design of waveguide magneto-optical isolators operating in 1.31 μm and 1.55 μm . *Opt. Express* **2007**, *15*, 639–645. [[CrossRef](#)] [[PubMed](#)]
22. Popkov, A.F.; Fehndrich, M.; Lohmeyer, M.; Dötsch, H. Nonreciprocal TE-mode phase shift by domain walls in magneto-optic rib waveguides. *Appl. Phys. Lett.* **1998**, *72*, 2508–2510. [[CrossRef](#)]
23. Fujita, J.; Levy, M.; Osgood, R.M., Jr.; Wilkens, L.; Dötsch, H. Polarization-independent waveguide optical isolator based on nonreciprocal phase shift. *IEEE Photonics Technol. Lett.* **2000**, *12*, 1510–1512. [[CrossRef](#)]
24. Pintus, P.; Pasquale, F.D.; Bowers, J.E. Integrated TE and TM optical circulators on ultra-low-loss silicon nitride platform. *Opt. Express* **2013**, *21*, 5041–5052. [[CrossRef](#)] [[PubMed](#)]
25. Ishida, E.; Miura, K.; Shoji, Y.; Yokoi, H.; Mizumoto, T.; Nishiyama, N.; Arai, S. Amorphous-Si waveguide on a garnet magneto-optical isolator with a TE mode nonreciprocal phase shift. *Opt. Express* **2017**, *25*, 452–462. [[CrossRef](#)]
26. Ghosh, S.; Keyvaninia, S.; Shirato, Y.; Mizumoto, T.; Roelkens, G.; Baets, R. Optical isolator for TE polarized light realized by adhesive bonding of Ce:YIG on silicon-on-insulator waveguide circuits. *IEEE Photonics J.* **2013**, *5*, 6601108. [[CrossRef](#)]
27. Shoji, Y.; Mizumoto, T. Waveguide magneto-optical devices for photonics integrated circuits. *Opt. Mater. Express* **2018**, *8*, 2387–2394. [[CrossRef](#)]
28. Yamaguchi, R.; Shoji, Y.; Mizumoto, T. Low-loss waveguide optical isolator with tapered mode converter and magneto-optical phase shifter for TE mode input. *Opt. Express* **2018**, *26*, 21271–21278. [[CrossRef](#)]

